Susceptibility of superconductor disks and rings with and without flux creep

Ernst Helmut Brandt
Max-Planck-Institut für Metallforschung, D-70506 Stuttgart, Germany
(Received 7 November 1996)

First some consequences of the Bean assumption of constant critical current J_c in type-II superconductors are listed and the Bean ac susceptibility of narrow rings is derived. Then flux creep is described by a nonlinear current-voltage law $E \propto J^n$, from which the saturated magnetic moment at constant ramp rate $\dot{H}_a(t)$ is derived for rings with general hole radius a_1 and general creep exponent n. Next the exact formulation for rings in a perpendicular applied field $H_a(t)$ is presented in the form of an equation of motion for the current density in thick rings and disks or the sheet current in thin rings and disks. This method is used to compute general magnetization curves $m(H_a)$ and ac susceptibilities χ of rings with and without creep, accounting also for nonconstant $J_c(B)$. Typical current and field (B) profiles are depicted. The initial slope of $m(H_a)$ (the ideal diamagnetic moment) and the field of full penetration are expressed as functions of the inner and outer ring radii a_1 and a. A scaling law is derived which states that for arbitrary creep exponent n the complex nonlinear ac susceptibility $\chi(H_0,\omega)$ depends only on the combination H_0^{n-1}/ω of the ac amplitude H_0 and the ac frequency $\omega/2\pi$. This scaling law thus connects the known dependencies $\chi=\chi(\omega)$ in the ohmic limit ($n=1$) and $\chi=\chi(H_0)$ in the Bean limit ($n\to\infty$). [S0163-1829(97)01921-8]

I. INTRODUCTION

The magnetic moment $\mathbf{m}=\frac{1}{2}\int \mathbf{r}\times\mathbf{J}(\mathbf{r})d^3r$ of a type-II superconductor is often calculated within the Bean model,[1,2] which assumes that the current density $\mathbf{J}(\mathbf{r})$ cannot exceed a critical value J_c, $J=|\mathbf{J}|\leq J_c$. If J locally exceeds J_c, the flux lines will rearrange such that $J\leq J_c$ again holds in the entire superconductor. An additional assumption disregards the reversible magnetization, or the finite lower critical field H_{c1}, by writing $\mathbf{B}=\mu_0\mathbf{H}$ inside (and outside) the material. Within this model, $\mathbf{m}$ depends only on the applied magnetic field H_a and on the geometry, i.e., on the sample shape and on the orientation of the applied field H_a. Being irreversible, $\mathbf{m}$ depends on the history of $H_a(t)$, but it does not depend explicitly on the time t. This means the rate $\dot{H}_a(t)$ at which the external field is increased or decreased does not enter the Bean model.

In experiments on high-T_c superconductors (HTSC's) the effects of flux creep often are not negligible. For example, when $H_a(t)$ is held constant, the magnetization may relax and will thus depend on the time t. As a consequence, when $H_a(t)$ is cycled, the predictions of the static Bean model may be observed at very slow sweep rates, while at high sweep frequencies deviations occur due to flux creep. This finding may appear counterintuitive since creep effects are expected to be more visible after longer time, i.e., at slow sweep rates. Our quanitative theory below explains this observation in terms of a scaling law which states that the same ac susceptibility is obtained at higher sweep frequency if the sweep amplitude is increased accordingly. Within continuum theory, flux creep effects originate from the nonzero resistivity of HTSC's occurring at sufficiently high temperatures and fields.

In this paper I investigate the influence of flux creep on the magnetization curves and nonlinear ac susceptibilities of superconducting disks and rings in a perpendicular field. In Sec. II some general features of the static Bean model are listed. The magnetization curves following from the Bean model for some basic longitudinal and transverse geometries are compiled in Sec. III. The nonlinear ac susceptibility of a narrow ring is given in Sec. IV. Flux creep effects and the saturation magnetization are discussed in Sec. V. Section VI presents exact equations of motion for the current density in thick disks and rings and for the sheet current in thin disks and rings; it is shown how these equations can be solved by matrix inversion and time integration; numerical results and approximate formulas are given for thin rings with arbitrary hole radius, namely, the initial slope of the magnetization curve and the field of full penetration in the Bean limit, from which approximate magnetization curves may be constructed. The exact magnetization curves for thin disks and rings are presented in Sec. VII, considering also flux creep and nonconstant critical current density $J_c(B)$ for sinusoidal applied field $H_a(t)$. From these hysteresis loops the nonlinear ac susceptibility $\chi(H_0)=\chi'-\chi''$ for disks and rings is calculated. The main results are summarized in Sec. VIII.

As a particularly useful result, a scaling law is derived in Sec. VI B, which applies to any power-law current-voltage curve $E\propto J^n$ (E is the electric field) and which states that for arbitrary creep exponent $n=\partial\ln E/\partial\ln J$ the susceptibility $\chi(H_0,\omega)$ depends only on the combination $H_0/\omega^{1/(n-1)}$ of the sweep amplitude H_0 and sweep frequency $\omega/2\pi$. This scaling connects the well-known facts that in the ohmic ($n=1$) or Bean ($n\to\infty$) limits χ depends only on ω or H_0, respectively.

II. FEATURES OF THE BEAN MODEL

Several general features follow from the Bean assumption of a static and field-independent J_c.

(i) When H_a is cycled between $-H_0$ and $+H_0$ the virgin curve $m(H_a)$ (with H_a increased from zero) determines the full hysteresis loop of m. The branches $m_\downarrow$ and $m_\uparrow$ in de-

creasing and increasing H_a read

$$m_{\downarrow}(H_a,H_0)=m(H_0)-2m\left(\frac{H_0-H_a}{2}\right),$$

$$m_{\uparrow}(H_a,H_0)=-m(H_0)+2m\left(\frac{H_0+H_a}{2}\right). \quad (1)$$

(ii) Only the ratios H_a/J_c, and H_0/J_c enter in Eq. (1). For general time-dependent $H_a(t)$ one may write

$$m[H_a(t)]=J_c\, l^4\, f[H_a(t)/lJ_c], \quad (2)$$

where l is a characteristic length of the specimen and f is a dimensionless function, see the examples below.

(iii) As noted recently,[3] for the Bean model the energy dissipated in the superconductor $U_{\rm diss}$ follows from $m(H_a)$ not only for a complete hysteresis cycle, where it is well known to be $U_{\rm diss}=\mu_0\oint H_a dm=\mu_0\oint m dH_a$, but for *any* point on the curve $m(H_a)$. The dissipated power $P=dU_{\rm diss}/dt\geqslant 0$ is

$$P=\int \mathbf{jE}\; d^3r=-\mu_0\dot{H}_a[m(H_a)-H_a m'(H_a)], \quad (3)$$

where $m'=dm/dH_a$. With $\partial/\partial t=\dot{H}_a\partial/\partial H_a$ one finds the dissipated energy $U_{\rm diss}$ along the virgin curve by time integrating $P=dU_{\rm diss}/dt=j_c\int E\; d^3r$,

$$U_{\rm diss}=\mu_0\int_0^{m(H_a)} H\; dm-\mu_0\int_0^{H_a} m\; dH$$

$$=\mu_0 H_a m(H_a)-2\mu_0\int_0^{H_a} m(H)\; dH. \quad (4)$$

Formula (4) means that $U_{\rm diss}$ is twice the area between the curve $m(H)$ and the straight line connecting the origin $m=H=0$ with the point $m(H_a)$. It appears that the relations (3) and (4) are restricted to the case of constant J_c; they were shown[3] to apply to all the basic Bean examples in longitudinal and transverse geometries listed below, but they do not apply to ohmic conductors. So far, I do not know a general proof.

(iv) In the Bean model the influence of the history of $H_a(t)$ is partly erased when H_a is cycled with increasing amplitude. In particular, for perodic $H_a(t)$ with slowly increasing amplitude, a Bean superconductor of arbitrary geometry ''remembers'' only the last cycle. It will be shown in Sec. VI that this property approximately holds even when strong creep occurs.

(v) The magnetic moment m does not depend explicitly on the time t. Therefore, m does not depend on the sweep rate or, if $H_a(t)$ is periodic, on the sweep frequency and also not on the shape of $H_a(t)$ (whether sinusoidal, square, trapezoidal, etc.). This property applies even when J_c depends on the magnetic field B. It just means that one considers the static response and neglects flux creep.

(vi) The static Bean model follows when a nonlinear current-voltage law $E(J)$ with a sharp bend at $J=J_c$ is assumed. A simple such model is to take the limit $n\to\infty$ in the power law

$$\mathbf{E(J)}=E_c\,(J/J_c)^n\mathbf{J}/J \quad (5)$$

with $J=|\mathbf{J}|$. This useful and realistic power law with finite creep exponent n will be used below to investigate creep effects, i.e., effects of finite resistivity.

When the exponent in Eq. (5) is $n<\infty$, the Bean properties (i) to (v) no longer apply. For $1\ll n<\infty$ the material law (5) leads to flux creep, i.e., a nonlinear, approximately logarithmic relaxation of $m(t)$ caused by a nonlinear diffusion of magnetic flux with J-dependent diffusivity $D(J)=E(J)/\mu_0 J$. With decreasing exponent n the creep becomes more pronounced. In the limit $n=1$, Eq. (5) describes an ohmic conductor, which exhibits linear diffusion of flux and exponential relaxation of $m(t)$. Note that for general n only the combination E_c/J_c^n enters in Eq. (5), and thus E_c (the voltage criterion) and J_c have no independent meaning. However, in the Bean limit $n\to\infty$ only J_c matters and the choice of E_c is irrelevant, while in the Ohmic limit $E/J=E_c/J_c=\rho$ is the constant resistivity and $D=\rho/\mu_0$ the usual flux diffusivity in ohmic conductors.

III. BEAN MAGNETIZATION CURVES FOR BASIC GEOMETRIES

A. Slab, cylinder, strip, disk

For later reference I list some basic examples for virgin magnetization curves. A large superconducting slab of width $2a$ and area A, and a long cylinder with radius a and length l, in a *parallel* field have the magnetic moments[1,2]

$$m_{\rm slab}=-J_c a^2 A(2h-h^2), \quad (6)$$

$$m_{\rm cyl}=-\pi J_c a^3 l(h-h^2+h^3/3) \quad (7)$$

for $0\leqslant h\leqslant 1$ with $h=H_a/H_p$, where $H_p=J_c a$ is the field of full penetration. For $H_a\geqslant H_p$, or $h\geqslant 1$, m stays constant since the current density has saturated to $J=J_c$ in the entire sample.

A thin strip[4–7] of width $2a$ and length $l\gg a$ and a circular disk[8–10] of radius a, both with thickness $d\ll a$, in a transverse field H_a have the magnetic moments

$$m_{\rm strip}(H_a)=-J_c d a^2 l\tanh h, \quad (8)$$

$$m_{\rm disk}(H_a)=-J_c d a^3\frac{2}{3}\left(\cos^{-1}\frac{1}{\cosh h}+\frac{\sinh|h|}{\cosh^2 h}\right) \quad (9)$$

for $0\leqslant h<\infty$ with $h=H_a/H_c$, where $H_c=J_c d/\pi$ for the strip and $H_c=J_c d/2$ for the disk. The two curves (8) and (9) differ by less than 0.012 if normalized to the same initial slope $m'(0)$ and same saturation value $m(\infty)$, cf. Fig. 1, where we plot the universal functions $f(x)=m_{\rm strip}/(-J_c d a^2 l)$ with $x=\pi H_a/J_c d$ and $f(x)=m_{\rm disk}/(-\pi J_c d a^3/3)$ with $x=8H_a/\pi J_c d$, which both exhibit $f'(0)=f(\infty)=1$ and almost coincide. The computed normalized Bean magnetic moment $m_{\rm square}(H_a)$ for a thin superconducting square[3,11,12] differs from $m_{\rm disk}(H_a)$ by less than 0.002.

In the considered limit $d/a\to 0$, the transverse moments $m_{\rm strip}(H_a)$ and $m_{\rm disk}(H_a)$ saturate only at infinitely large field H_a. With finite thickness d the magnetic saturation is reached when the flux and current front, which is positioned

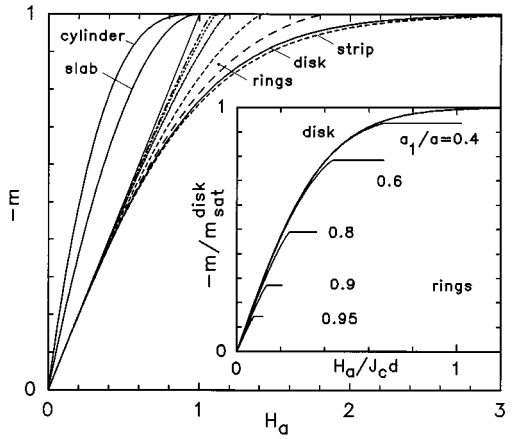

FIG. 1. Bean magnetization curves $m(H_a)$ for a thin strip [Eq. (8)] and disk [Eq. (9)], and for rings with radius ratios $a_1/a=0.4$, 0.6, 0.8, 0.9, and 0.95 in perpendicular field H_a. The curves are normalized to unity initial slope and unity saturation value by plotting $m(H_a)/m_{\rm sat}$ versus $H_a m'(0)/m_{\rm sat}$. Also shown is $m(H_a)/m_{\rm sat}$ for long slabs [Eq. (6)] and cylinders [Eq. (7)] in parallel field, plotted versus H_a/H_p to avoid crossing of curves. The inset shows $m(H_a)$ for these rings and the disk in constant units $m_{\rm sat}^{\rm disk}=\pi J_c d a^3/3$ for m and $J_c d$ for H_a, which show how the magnetic saturation is reached earlier with increasing hole radius a_1. The ring data were computed using a creep exponent $n=101$.

at $x_p=r_p=a/\cosh h$, has penetrated to a distance $\approx d/2$ from the center $x=0$ or $r=0$, i.e., to $x_p=r_p\approx d/2$. More precisely, one finds from analytical calculations[13] the penetration fields[14] for $d\ll a$,

$$H_p^{\rm strip}=J_c\frac{d}{\pi}\left[1+\ln\frac{2a}{d}\right], \tag{10}$$

$$H_p^{\rm disk}=J_c\frac{d}{2}\left[2+\ln\frac{2a}{d}\right]. \tag{11}$$

The prefactors in Eqs. (10) and (11) are the above defined critical fields of strips and disks, $H_c=J_c d/\pi$ and $H_c=J_c d/2$. Above the penetration fields (10) or (11) the magnetic moment saturates to the values $m_{\rm sat}^{\rm strip}=J_c d a^2 l$ and $m_{\rm sat}^{\rm disk}=J_c d a^3\pi/3$.

B. Narrow ring

The cutoff problem for H_p does not arise if the central part of the strip or disk is removed. The magnetic moment of the resulting double strip (with connected ends) or ring then saturates naturally, with the penetration field H_p and the saturated magnetic moment depending on the width or radius of the cut-out slit or hole. For the thin double strip the Bean magnetic moment $m(H_a)$ in principle may be calculated by conformal mapping as suggested in Ref. 6. For both the double strip and the ring the numerical method of Refs. 15–20 may be used to compute the flux penetration and the magnetic moment, cf. Sec. VI.

First I discuss the limit of a thin narrow ring with width w much smaller than the mean radius R, $a_1=R-w/2\leqslant r\leqslant R+w/2=a$. The virgin magnetization curve of such a ring is composed of two straight lines,

$$m_{\rm ring}(H_a)=-(H_a/H_p^{\rm ring})m_{\rm sat},\quad H_a\leqslant H_p^{\rm ring},$$

$$m_{\rm ring}(H_a)=-m_{\rm sat},\quad H_a\geqslant H_p^{\rm ring}. \tag{12}$$

This is so since the screening supercurrent in the ring is limited to a maximum value $I_c=J_c d w$. As long as the current I induced in the ring by the applied field H_a is $|I|<I_c$, no magnetic flux can penetrate through the ring into the hole of the ring. When $|I|=I_c$ is reached, the ring becomes transparent to magnetic flux. Therefore, when the applied field is increased further, flux lines will move through the ring as described in Refs. 6 and 7, which treat the superconducting strip with transport current in an applied field, see also the flux profiles in Fig. 10 below. The flux lines transport magnetic flux into the ring hole until the screening current has decreased again to the value I_c. The magnetic moment $m=\pi R^2 I$ of the ring thus saturates to the value

$$|m|\leqslant m_{\rm sat}=\pi R^2 I_c. \tag{13}$$

The applied field value H_p at which this saturation is reached follows from the inductivity L of the flat ring,[21]

$$L=\mu_0 R\left(\ln\frac{8R}{w}-c\right) \tag{14}$$

where $c=1/2$. For comparison, the inductivity of a ring made of a wire with diameter $w\ll R$ is also given by formula (14) but with $c=2$.[22,21] Our computation in Sec. VII finds that for a flat superconducting ring one actually has $c=0.614$ in formula (14). This is so because the result $c=1/2$ assumes uniform current density across the ring, while the real current distribution is peaked at the edges of the ring.[6,7] In the limit $w\ll R$ the sheet current J_s in a superconducting ring behaves as in a straight thin strip, $J_s(r)=(I/\pi)(w^2/4-x^2)^{-1/2}$ with $x=r-R$. Therefore, when flux penetrates the conductor of a flat ring, the constant decreases from $c=0.614=2-\ln 4$ at $H_a=0$ to $c=1/2$ (or $c=0.307=1-\ln 2$, see Sec. VII B) at $H_a\geqslant H_p^{\rm ring}$. For simplicity one may put $c\approx 1/2$ in the next three formulas.

The magnetic flux generated in the ring hole by a ring current I is $\phi=LI$. As long as $I<I_c$ one has ideal screening, thus $\phi=-\pi R^2\mu_0 H_a$. Equating these two fluxes one obtains for the flat ring

$$I=\phi/L=-\frac{\pi R}{\ln(8R/w)-c}H_a. \tag{15}$$

At $H_a=H_p$ one has reached $|I|=I_c=J_c w d$, thus

$$H_p^{\rm ring}=\frac{\ln(8R/w)-c}{\pi R}I_c. \tag{16}$$

The slope of $m(H_a)$ for $H_a<H_p$ is therefore

$$m'_{\rm ring}(0)=-\frac{m_{\rm sat}}{H_p^{\rm ring}}=-\frac{\pi^2 R^3}{\ln(8R/w)-c}. \tag{17}$$

Comparing this with the ideal diamagnetic moment of the disk obtained from Eq. (9),

$$m'_{\rm disk}(0)=-8a^3/3, \tag{18}$$

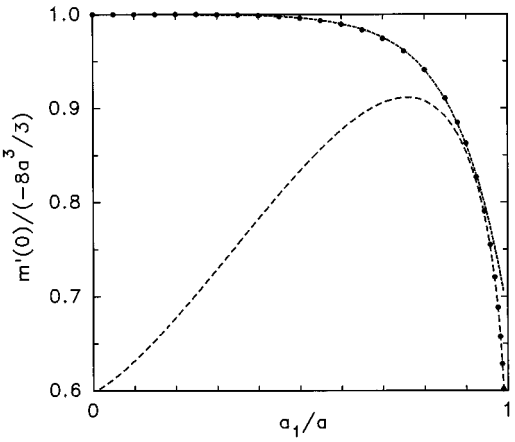

FIG. 2. The initial slope $m'(0)$ of the magnetization curve of a nonlinear conductor or a superconductor ring versus the ratio $x=a_1/a$ of the inner and outer radius. This is also the magnetic moment of an ideal diamagnet in unit applied field. The dots denote the computed values, see Table I. The dotted and dashed lines give the approximations (42) for small and large x.

one finds the remarkable result that a ring has a slightly smaller ideal diamagnetic moment than a disk of the same outer radius $a=R+w/2\gg w$, although the flux expelled from the ring and disk is the same, $\pi a^2\mu_0 H_a$.

The initial slope $m'_{\rm ring}(0)$ and the penetration field $H_p^{\rm ring}$ are computed below in Sec. VII for superconducting rings with arbitrary inner radius $0\leqslant a_1<a$. The results, depicted in Figs. 2 and 3, show that the expressions (16) with $c=0.307=1-\ln 2$ and (17) with $c=0.614=2-\ln 4$ are excellent approximations with a relative deviation of less than 2% for $a_1/a>0.8$. Figure 1 shows that the magnetization curves of wide rings are no longer straight lines but are slightly curved and merge with the curve for the disk when $a_1\to 0$.

IV. SUSCEPTIBILITY OF NARROW RINGS

With the prescription (1) the virgin magnetization curve (12) yields hysteresis loops in the shape of parallelograms.[23–25] From these loops one obtains the complex susceptibility $\chi=\chi'-i\chi''$ of a superconducting narrow ring with constant J_c. For cycled magnetic field $H_a(t)=H_0\sin(\omega t)$ one may define[26,27]

$$\chi(H_0)=\frac{\omega}{\pi H_0}\int_0^{2\pi} m(t)\; e^{-i\omega t}\; dt\;. \tag{19}$$

Note that this *nonlinear* susceptibility does not depend on the frequency $\omega/2\pi$ if $m(t)$ is taken from the Bean model, but it depends on the sweep amplitude H_0. In contrast, the *linear* susceptibility of an ohmic conductor or of any conductor with linear complex resistivity (e.g., a superconductor above the depinning line) depends on ω but not on H_0. One may also consider the higher harmonic responses χ_ν, $\nu=2,3,4,\ldots$, by replacing in Eq. (19) $\exp(-i\omega t)$ by $\exp(-i\nu\omega t)$. Here I shall consider the fundamental response $\chi=\chi_1(H_0)$ and the strongest harmonics $\chi_3(H_0)$. The susceptibilities $\chi_\nu(H_0)$ for thin disks are given by Clem and Sanchez.[10]

From Eqs. (1), (12), and (19) one obtains the susceptibility of the ring normalized to the initial value $\chi(0)=-1$, i.e., to $\chi\to\chi/|m'(0)|$,

$$\chi'(h)=-1,\quad \chi''(h)=0,\quad h\leqslant 1,$$

$$\chi'(h)=-\frac{1}{2}-\frac{1}{\pi}\arcsin s-\frac{1}{\pi}s\,\sqrt{1-s^2}\;,$$

$$\chi''(h)=\frac{4}{\pi}\,\frac{h-1}{h^2}=\frac{1-s^2}{\pi},\quad h\geqslant 1, \tag{20}$$

with $h=H_0/H_p$ and $s=2/h-1$, see Fig. 4 (top).

Interestingly, with the ring susceptibility (20) the polar plot χ'' versus χ' with h as a parameter is *symmetric*, i.e., $\chi''(\chi')$ yields the same curve as $\chi''(-1-\chi')$. Figure 4 (bottom) shows these polar plots for the ring and for the disk and strip. The maximum of the dissipative part of the ring susceptibility $\chi''_{\rm max}=1/\pi=0.318$ occurs at $h=2$ (at $s=0$). For large amplitudes $h=H_0/H_p\gg 1$ one has $\chi'(h)\approx -1.69/h^{3/2}$ and $\chi''(h)\approx 4/\pi h$.

The $\chi(H_0)$ for disks and strips differ by less than 0.010 (χ') or 0.0043 (χ''), and $\chi(H_0)$ for thin squares and disks differ by less than 0.001. The maximum $\chi''_{\rm max}=0.240\,771$ (0.236 466) for the disk (strip) occurs at $x=8H_0/\pi J_c d=2.4738$ or $x=\pi H_0/J_c d=2.4642$; for these field units see the discussion below Eq. (9). For large amplitudes $x\gg 1$ one has $\chi'\approx 1.910/x^{3/2}$ ($1.930/x^{3/2}$) for disks (strips) and $\chi''\approx 4/\pi x$ for both. This means that the large amplitude behavior of $\chi(H_0)$ is very similar for rings, disks, and strips, if the amplitude H_0 is expressed in the reduced units of Fig. 1, which yield unity initial slope and unity saturation of $m(H_a)$.

A further remarkable property of the ac response of a narrow ring within the Bean model is that the absolute value of χ_3 is related to the dissipative part of χ, Eq. (20), by $|\chi_3(H_0)|=\frac{1}{3}\chi''(H_0)$. This exact coincidence was also noted by Ishida and Mazaki,[24] who proved it theoretically and found nice agreement with experiments. For higher harmon-

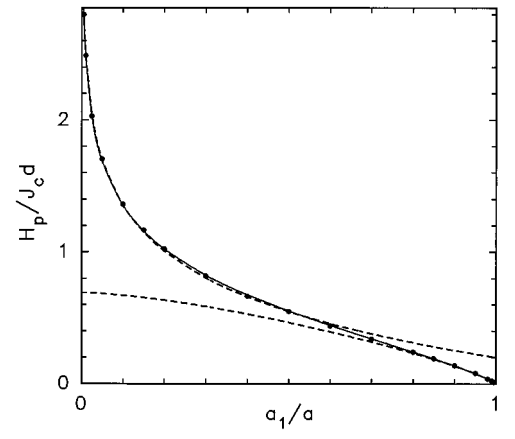

FIG. 3. The field of full penetration H_p of thin superconductor rings in the Bean model with constant critical current density J_c plotted versus the ratio $x=a_1/a$ of the inner and outer radius. The dots denote the computed values, see Table I. The dashed lines show the approximations (48) for small and large x, and the solid line the expression (49).

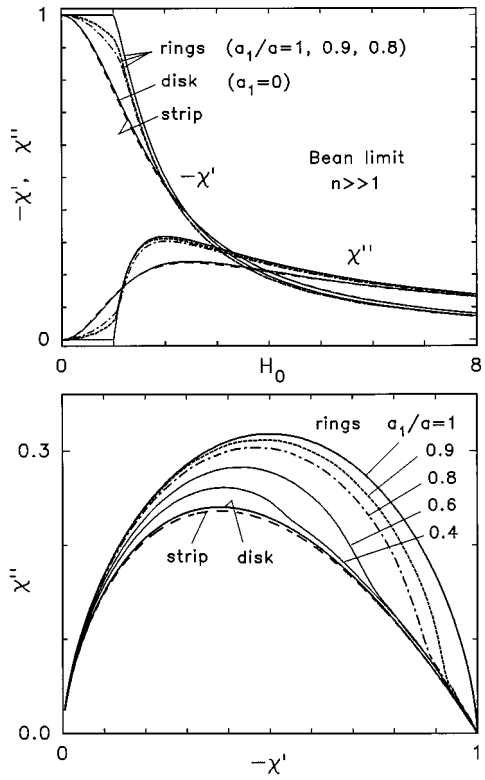

FIG. 4. Top: Real and imaginary parts of the complex susceptibility $\chi(H_0)=\chi'-i\chi''$ of thin strips, disks, and rings with various radius ratios a_1/a plotted versus the amplitude H_0 of the ac field in the Bean model with constant J_c. The unit of H_0 is $J_c d/\pi$ for the strip and $\pi J_c d/8$ for the disk. For rings H_0 is in units of a penetration field $H_p'\approx H_p$ which gives best fit to the sharp rise in the ideal ring χ'': $H_p'/J_c d=0.126$ (0.210) for $a_1/a=0.9$ (0.8), while from Table I one has $H_p/J_c d=0.136$ (0.239). For $a_1/a\to 1$ one finds $H_p'/H_p\to 1$. Bottom: Polar plots of the same $\chi=\chi'-i\chi''$. For the narrow (not necessarily thin) ring χ' and χ'' [Eq. (20)] are discontinuous at $H_0=H_p$ and the polar plot is symmetric.

ics $\nu=5$, 7,..., a similar relationship does not apply. We will see in Sec. VIII below that this property is lost when flux creep is allowed for.

For comparison with the Bean limit $n\to\infty$ shown in Fig. 4, the complex susceptibility for disks and various rings is depicted in Fig. 5 for finite creep exponents $n=3$, 5, 11, 51, and 201. These curves were computed by the method of Sec. VI using the current-voltage power law (5) and $\omega=2E_c/(\mu_0 J_c d a)$. Note that with increasing hole radius a_1, a bend develops in the curves $\chi'(H_0)$, $\chi''(H_0)$, and $\chi''(-\chi')$ at $H_0\approx H_p$. This bend is sharpest in the Bean limit $n\to\infty$ but it dissapears for strong creep, $n\leqslant 5$. The tiny wiggles of χ' and χ'' at $H_0\ll H_p$ are artifacts caused by the spatial grid used for the computation, but the bends near H_p are real. At small amplitudes $H_0<H_p$, χ' and χ'' for rings with finite width deviate considerably from the narrow ring Bean limit ($\chi'=-1$, $\chi''=0$) even for large n.

V. EFFECTS OF FINITE RESISTIVITY

Within a continuum description the phenomenon of flux creep is caused by the finite resistivity of the superconductor or of any conductor with a nonlinear current-voltage curve $E(J)$ with positive curvature. Various $E(J)$ laws were suggested based on microscopic models. For example, the collective creep[28] and vortex glass pictures[29] yield a current-density-dependent activation energy for thermally activated depinning,

$$U(J)=U_0[(J_c/J)^{\alpha}-1]/\alpha \tag{21}$$

with $\alpha>0$.[28–30] Inserting this into the Arhennius law

$$E(J)=E_c\exp[-U(J)/kT] \tag{22}$$

one obtains a highly nonlinear resistivity $\rho(J)=E(J)/J$. In the limit $\alpha\ll 1$, Eq. (21) becomes $U(J)\approx U_0\ln(J_c/J)$, yielding with Eq. (22) $E(J)=E_c\exp[-U(J)/kT]=E_c(J/J_c)^{U_0/kT}$. This is the power law, Eq. (5), with $n=U_0/kT$. Such a power law, or a logarithmic $U(J)$, or a small glass exponent $\alpha\ll 1$, is often observed in experiments.

The power law (5) is very convenient for analytical calculations[31–36] and for computations.[3,14–21] In creep experiments where the ramping of $H_a(t)$ is stopped at time $t=0$ one obtains after some transient time τ the universal relaxation[33–36] $E\propto(\tau/t)^{n/(n-1)}\approx\tau/t$ and $m(t)\propto J\propto(\tau/t)^{1/(n-1)}\approx 1-[1/(n-1)]\ln(t/\tau)$ if $n\gg 1$. In the ohmic limit $n=1$ one has $m(t)\propto J\propto E\propto\exp(-t/\tau)$.

In Eq. (5) general dependences $J_c=J_c(B)$ and $n=n(B)$ are allowed. Of course, further dependences on temperature and on any other spatially constant parameter are also allowed, as in the original Bean model. Static ($n\to\infty$) extensions of the Bean model to $J_c=J_c(B)$ have often been considered,[2,37] but also dynamic computations with creep, using Eq. (5) with $n<\infty$, present no difficulty.[18,19] Superconductors with inhomogeneous pinning, produced, e.g., by partial irradiation, are easily modeled by using a space dependent $J_c(\mathbf{r})$.[19,20]

One can easily calculate the fully penetrated state which is reached after sufficiently long time $t\to\infty$ during constant ramp rate $\dot{H}_a$. In this stationary state the current has saturated, thus the current-caused magnetic field does not change any more, and the electric field $\mathbf{E}_{\rm sat}$ follows from $\nabla\times\mathbf{E}_{\rm sat}=-\dot{\mathbf{B}}=-\dot{\mathbf{B}}_a$, where $\mathbf{B}_a=\mu_0\mathbf{H}_a$. This very general law applies to any geometry and specimen shape. For disks and rings this means

$$\mathbf{E}_{\rm sat}=\hat{\varphi}\dot{B}_a\frac{r}{2}, \tag{23}$$

where $\hat{\varphi}$ is the azimuthal unit vector and $B_a=\mu_0 H_a$. From the current-voltage law (5), which inverted reads $\mathbf{J}=J_c\,(E/E_c)^{1/n}\mathbf{E}/E$, one obtains with Eq. (23)

$$\mathbf{J}_{\rm sat}=\hat{\varphi}\left(\frac{\dot{B}_a a}{2E_c}\right)^{1/n}\left(\frac{r}{a}\right)^{1/n}. \tag{24}$$

The saturated magnetic moment of a ring with outer radius a, inner radius $a_1=a-w$, and thickness d is thus

$$|m|\leqslant m_{\rm sat}=d\pi\int_{a_1}^{a}r^2J(r)\,dr, \tag{25}$$

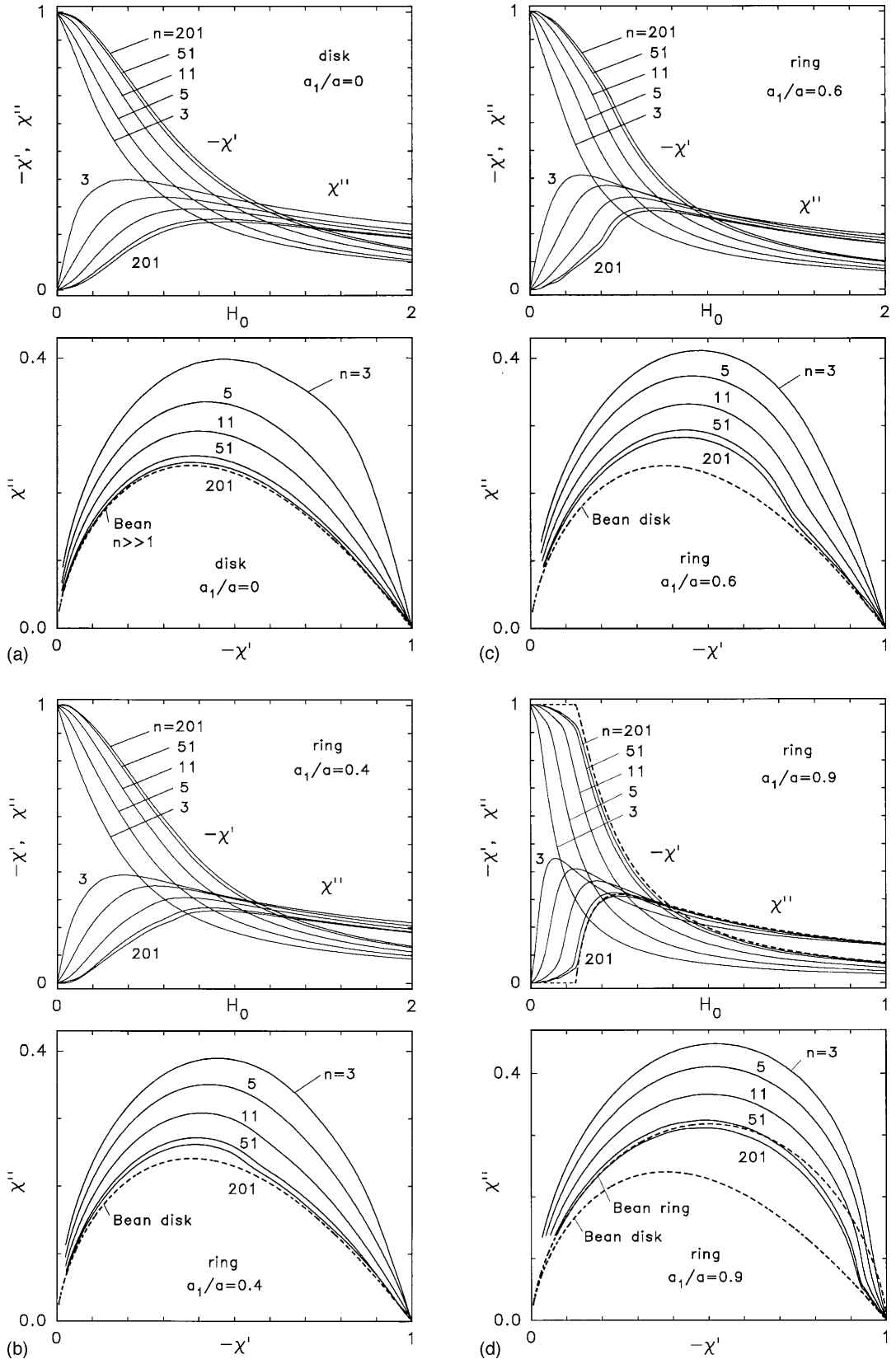

FIG. 5. (a) Top: Real and imaginary parts of the nonlinear complex susceptibility $\chi(H_0)=\chi'-i\chi''$ of a thin disk plotted versus the ac amplitude H_0 for various creep exponents $n=3$, 5, 11, 51, and 201 in $E=E_c(J/J_c)^n$ with constant J_c. H_0 is in units $J_c d$. Bottom: Polar plots of the same $\chi=\chi'-i\chi''$. The dashed line shows the Bean model $n\to\infty$ for the disk. (b) Same as (a) but for a wide ring with radius ratio $a_1/a=0.4$. (c) Ring with $a_1/a=0.6$. (d) Ring with $a_1/a=0.9$. The dashed curves show χ' and χ'' for the narrow Bean ring with $a_1/a\to 1$ and for the disk; for the field units see the caption of Fig. 4.

$$m_{\rm sat}=\frac{\pi\ n}{3n+1}J_c a^3 d\left[1-\left(\frac{a_1}{a}\right)^{3+(1/n)}\right]\left(\frac{\dot B_a a}{2E_c}\right)^{1/n}.$$

In the Bean limit $n\to\infty$ the first factor in Eq. (25) reduces to $\pi/3$ and the last factor becomes unity, i.e., the ramp rate $\dot B_a$ and voltage criterion E_c do not enter. One then obtains the well-known exact Bean result

$$m_{\rm sat}=\frac{\pi}{3}J_c d(a^3-a_1^3)=\pi R^2 I_c\left(1+\frac{3w^2}{4R^2}\right), \qquad (26)$$

cf. Eq. (13) and Fig. 1. When flux creep is considered ($n<\infty$), the saturation value (25) is reduced or enhanced with respect to the Bean limit, depending on whether the ramp rate $\dot B_a$ is less than or larger than the value $[3+(1/n)]^n 2E_c/a$. However, this criterion depends on the voltage criterion and thus on the definition of $J_c=J(E_c)$. In principle, J_c may be defined such that $m_{\rm sat}/J_c$ stays independent of n or of $\dot B_a$. Moreover, I will show in Sec. VI B that the basic equations of this problem and thus all its solutions, are invariant with respect to the simultaneous change of the scales of time by a factor C, and of current and magnetic field by a factor $C^{1/(n-1)}$.

As shown in Ref. 14, the magnetic saturation is reached exponentially in time,

$$m_{\rm sat}-|m|\propto\exp(-t/\tau)\ ,$$

$$\tau=\text{const}(\mu_0 J_c a/n\dot B_a)(\dot B_a a/E_c)^{1/n}, \qquad (27)$$

where const~ 1 follows from an eigenvalue problem. This means that in spite of creep the saturation typically is reached quite fast when the ramp rate is constant.

We will see in Sec. VII C that when $B_a(t)$ is cycled sinusoidally, the magnetic moment $m(t)$ starts to decrease already *before* $B_a(t)$ has reached its maximum. This *decrease* of $|m(t)|$ during *increasing* applied field $B_a(t)=B_0\sin\omega t$ was ascribed to flux creep, which dominates when the ramp rate $\dot B_a(t)=B_0\omega\cos\omega t$ becomes sufficiently small. However, a more appropriate quantitative interpretation[38] ascribes this decrease of $|m|$ to the decreasing ramp rate $|\dot B_a|$. Namely, when the current density J has nearly saturated, the electric field decreases like the ramp rate, $|E|\approx|(r/2)\dot B_a|$, thus also $|J|=J_c|E/E_c|^{1/n}$ decreases, and $m=m(\dot B_a)$ is given by the ramp-rate-dependent saturation value, Eq. (25).

VI. EXACT FORMULATION FOR RINGS

A. Equation of motion for J

The equation of motion for the current density $J(\mathbf{r},t)$ in disks and rings in an axial magnetic field $B_a(t)$ is obtained by generalizing the expressions for disks of finite thickness[14] or for thin disks[17–20] with $d\ll a$. For thick rings with $a_1\le r\le a$, $-d/2\le z\le d/2$ this equation reads

$$\dot J(\mathbf{r},t)=\mu_0^{-1}\int_{a_1}^{a}dr'\int_0^{d/2}dz'\ Q(\mathbf{r},\mathbf{r}')^{-1}f(\mathbf{r}',t)\ ,$$

$$f(\mathbf{r},t)=J(\mathbf{r},t)^n\frac{E_c}{J_c^n}-\frac{r}{2}\dot B_a(t)\ . \qquad (28)$$

Here $\mathbf{r}=(r,z)$, $r=(x^2+y^2)^{1/2}$, $f(\mathbf{r},t)$ is the electric field which drives the current (the emf induced by the varying applied field, minus the voltage drop), and $Q(\mathbf{r},\mathbf{r}')^{-1}$ is the inverse of the (negative) integral kernel

$$Q(\mathbf{r},\mathbf{r}')=q(r,r',z-z')+q(r,r',z+z')\ ,$$

$$q(r,\zeta)=\int_0^{\pi}\frac{d\varphi}{2\pi}\frac{r'\cos\varphi}{(\zeta^2+r^2+r'^2+2rr'\cos\varphi)^{1/2}}\ . \qquad (29)$$

The inversion of this kernel may be acieved by tabulating it on a two-dimensional grid and inverting the resulting matrix.[14] The flux and field profiles and magnetization curves for disks computed from Eq. (28) look very similar[39] to the results for superconducting bars with the same rectangular cross section $d\times 2a$ in a perpendicular field, which are depicted in Ref. 14.

For thin disks and rings with $d\ll a$ one may average $J(r,z)$ over the specimen thickness, defining the sheet current $J_s(r)=\int_{-d/2}^{d/2}J(r,z)dz$. The equation of motion (28) then reduces to an equation for $J_s(r,t)$ in a ring,

$$\dot J_s(r,t)=\mu_0^{-1}\int_{a_1}^{a}dr'\ Q(r,r')^{-1}f_s(r',t)\ ,$$

$$f_s(r,t)=J_s(\mathbf{r},t)^n\frac{E_c}{(J_c d)^n}-\frac{r}{2}\dot B_a(t)\ , \qquad (30)$$

where $Q(r,r')^{-1}$ is the inverse of the kernel (29) taken at $z=z'=0$,

$$Q(r,r')=\int_0^{\pi}\frac{d\varphi}{\pi}\frac{r'\cos\varphi}{(r^2+r'^2+2rr'\cos\varphi)^{1/2}}\ . \qquad (31)$$

The equations of motion (28) and (30) are very convenient for the calculation of the penetration and exit of flux by starting with $B_a=0$, $J=0$, and then increasing $B_a(t)$ either with constant $\dot B_a$ or by cycling $B_a(t)$. If $B_a(t)$ is held at a constant value, genuine flux creep can be calculated from Eqs. (28) and (30) over many decades in the time t.[3] Exact solutions have been obtained for flux creep[34–36] and for the linear ac response during flux creep in longitudinal[40] and transverse[41] geometries.

Note that all these computations of the current density $J(r,z,t)$ or sheet current $J_s(r,t)$, and the calculation of the magnetic moment of the disk or ring,

$$m=\pi\int_{a_1}^{a}dr\ r^2\int_{-d/2}^{d/2}dz\ J=\pi\int_{a_1}^{a}dr\ r^2\ J_s, \qquad (32)$$

did not require computation of the magnetic field. This means no spatial derivatives have to be computed, and fields outside the specimen do not enter and thus do not have to be cut off or fit to some boundary conditions at some artificial far-away boundary. In our method all integrations are restricted to the current-carrying specimen volume. This

method is thus very effective both for numerical computations and for analytical calculations, see Refs. 14,15,17, 34,36,41.

After the currents have been calculated from Eqs. (28) or (30), the magnetic field inside and outside the specimen can be obtained by the Biot-Savart law. Writing $\mathbf{B}=\mathrm{rot}\mathbf{A}+\mathbf{B}_a$ with $\mathbf{A}=\hat{\varphi}A(r,z)$, one gets the components $B_z=\partial A/\partial r+A/r+B_a$ and $B_r=-\partial A/\partial z$ with

$$A(\mathbf{r})=-\mu_0\int_{a_1}^{a}dr'\int_0^{d/2}dz'\;Q(\mathbf{r},\mathbf{r}')J(\mathbf{r}')\;. \qquad (33)$$

For a thin disk or ring one has at the surfaces $z=\pm d/2\ll a$ the field components $B_z=\partial A(r,0)/\partial r+A(r,0)/r+B_a$ and $B_r=\mp J_s(r)/2$ (since the jump of the parallel component B_r equals the sheet current J_s) with

$$A(r)=-\mu_0\int_{a_1}^{a}dr'\;Q(r,r')J_s(r')\;. \qquad (34)$$

B. Scaling of frequency and amplitude

When a power law is assumed for the current-voltage curve, $E\propto J^n$ or $\rho=E/J\propto J^\sigma$ with $\sigma=n-1$, cf. Eqs. (5) and (22), then the equations of motion (28) and (30) for the currents in thick and thin disks or rings (and in all other geometries) possess a remarkable scaling property. Namely, when one changes the time units by a constant factor of C and the current and field units by a factor of $C^{1/\sigma}$, where $\sigma=n-1$, then these equations are invariant, i.e., the same solutions result for these scaled quantities. Explicitly, if the equation for the current density $J(\mathbf{r},t)$ is expressed in terms of $\tilde{t}=t/C$ then the new functions

$$\tilde{J}(\mathbf{r},\tilde{t})=J(\mathbf{r},t)C^{1/\sigma},\quad \tilde{B}_a(\tilde{t})=B_a(t)C^{1/\sigma} \qquad (35)$$

satisfy the same equation of motion. The resulting magnetic field $\tilde{\mathbf{B}}$ and magnetic moment $\tilde{m}$ scale by the same factor as J,

$$\tilde{\mathbf{B}}(\mathbf{r},\tilde{t})=\mathbf{B}(\mathbf{r},t)C^{1/\sigma},\quad \tilde{m}(\tilde{t})=m(t)C^{1/\sigma}\;. \qquad (36)$$

In particular, for periodic $B_a(t)=B_0\sin\omega t$, the resulting complex susceptibility $\chi(B_0,\omega)$ normalized to $\chi(0,\omega)=\chi(B_0,\infty)=-1$, i.e., to the ideal diamagnetic limit occurring at zero amplitude or infinite frequency, remains *unchanged* if one increases, e.g., ω by a factor of 10 and B_0 by a factor of $10^{1/\sigma}$. The resulting magnetic moment is then larger by the same factor of $10^{1/\sigma}$ as is also the applied field B_a. Therefore, the shape of the hysteretic magnetization curve $M(B_a)$ remains unchanged and also the polar plots $\chi''(\chi')$ of $\chi=\chi'-i\chi''$.

For periodic $B_a(t)$ this scaling law states that the normalized $\chi(B_0,\omega)$ and the shape of the hysteresis loop $m(B_a)$, depend only on the combination $B_0/\omega^{1/\sigma}$ or on ω/B_0^σ. This general statement connects the two limiting cases of ohmic conductors, exhibiting $\sigma=0$ and thus $\chi=\chi(\omega)$, and of Bean superconductors, exhibiting $\sigma\to\infty$ and thus $\chi=\chi(B_0)$.

C. Computational method

From Eqs. (30) to (34) one may compute the sheet current, the irreversible magnetization curves, and the magnetic field in and around thin disks and rings with material laws $\mathbf{B}=\mu_0\mathbf{H}$ and $\mathbf{E}=E_c\,|J/J_s|^n\mathbf{J}/J$ (5) in a perpendicular $B_a(t)$. Since these equations are one dimensional in space, the numerical program is very fast and accurate if the following tricks are considered

(i) For the spatial integration a nonequidistant grid r_i may be chosen which has vanishing spacing (or vanishing weights $w_i=dr_i/di$) at the inner and outer edges $r=a_1$ and $r=a$, e.g., $r_i=a_1+(3u_i^2-2u_i^3)(a-a_1)$, $w_i=6\,u_i(1-u_i)(a-a_1)/N$, with $u_i=(i-\frac{1}{2})/N$, $i=1,2,\ldots N$, $N\approx 10$ to 100. For the computation of $J_s(r)$ only grid points inside the ring are required, $a_1\leqslant r_i\leqslant a$. The subsequent computation of $B_z(r_j)$ may also use grid points in the ring hole and outside the ring in the plane $z=0$. In principle, $B_z(r,z)$ and $B_r(r,z)$ may be calculated also outside the disk plane by using a two-dimensional grid $\mathbf{r}_j=(r,z)_j$ and the kernel $Q(\mathbf{r},\mathbf{r}')$ (29).

(ii) Integrals over any function defined in the interval $a_1\leqslant r\leqslant a$ may be evaluated as a weighted sum, e.g., writing $f_i=f(r_i)$ and $F_i=F(r_i)$,

$$\int_{a_1}^{a}Q(r_i,r')f(r')\;dr'\approx\sum_{j=1}^{N}Q_{ij}w_jf_j=F_i\,. \qquad (37)$$

(iii) When tabulated on the grid r_i the kernel $Q(r,r')$ becomes a two-dimensional matrix $Q_{ij}=Q(r_i,r_j)$. The inverse kernel $Q(r,r')^{-1}$ is the inverse of this matrix if equidistant grid points (constant weights w_i) are used. For a general grid one has to invert this matrix times the weights w_i, $(Q^{-1})_{ij}=(Q_{ij}w_j)^{-1}$ as can be seen by inverting Eq. (37),

$$f_i=\sum_{j=1}^{N}\;(Q_{ij}w_j)^{-1}F_j\,. \qquad (38)$$

(iv) The time step dt used for the time integration of $\dot{J}$ should be chosen as $dt=c_1/[\max(\rho)+c_2]$, where $\rho=E/J=(E_c/J_c)\,|J/J_c|^{n-1}$ and c_1 and c_2 are constants. A finite c_2 is required to limit the time step at the moment when the ramp rate $\dot{B}_a(t)$ changes sign.

D. Current and field profiles

Figures 6 to 9 show the sheet current $J_s(r)$ and the corresponding magnetic field profiles $B(r)=B_z(r)$ in the specimen plane $z=0$, computed for the thin disk ($a_1=0$) and for a wide ($a_1/a=0.4$) and a narrow ($a_1/a=0.8$) ring. Shown are the Bean limit ($n=101$, Fig. 6) with $J_c=\mathrm{const}$ in increasing (Fig. 6) and decreasing (Fig. 9) field B_a. Also shown is an example with field-dependent critical current $J_c(B)=J_c(0)/(0.8+|B|)$ (Kim model, Fig. 7, J_s and B/μ_0 in units J_cd) and one case with strong creep $n=9$ (Fig. 8). Note that in Fig. 9 in decreasing $B_a(t)$ the J_s profiles (but not the B profiles) nearly coincide with the J_s profiles of Fig. 6 in increasing $B_a(t)$, multiplied by -2 and then shifted up by $+J_c$, as it should be in the Bean model,[1,2,5,9] see also Eq.

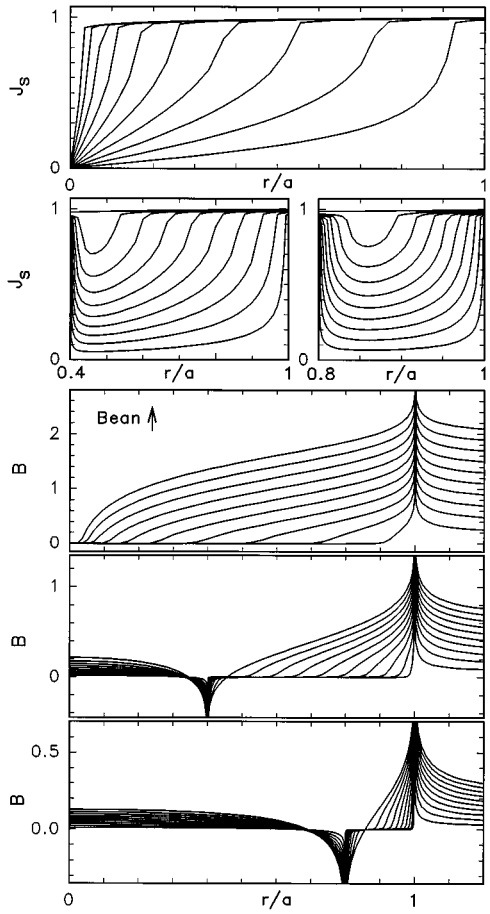

FIG. 6. Profiles of the sheet current $J_s(r)$ (top) and the perpendicular magnetic field $B=B_z(r)$ in the specimen plane (bottom) in a disk and in rings with radius ratios $a_1/a=0.4$ and 0.8 during flux penetration in an increasing applied field $H_a(t)$. The ten depicted curves are for $H_a/H_p=0.1,0.2,\ldots,1$ with the penetration field $H_p=2J_cd$ for the disk chosen arbitrarily and $H_p=0.6699J_cd$ $(0.2389J_cd)$ for the two rings taken from Table I. Bean model with $J_c=$ const, $n=101$, J_s is in units J_cd and B in units μ_0J_cd. A grid of 40 nonequidistant points $a_1<r_i<a$ was used.

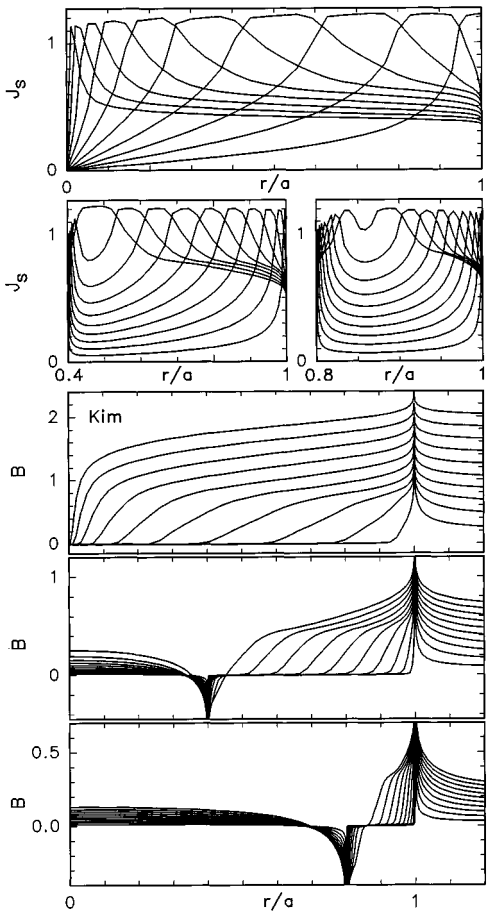

FIG. 7. Same as Fig. 6 but for field-dependent critical sheet current $J_s(B)=J_s(0)/(0.8+|B|)$ (Kim model) with J_s and $H=B/\mu_0$ in units J_cd.

(1). For stronger creep (Fig. 8) the corners of the J_s profiles become rounded but not the B profiles.

VII. MAGNETIZATION CURVES

A. Initial slope

The initial slope of the magnetization curve $m'_{\rm ring}(0)$ with the limits (17) $(a_1/a\to1)$ and (18) $(a_1/a\to0)$, for arbitrary radius ratio a_1/a may be directly obtained from the inverted matrix $Q(r,r')^{-1}$ in the following way. Inverting Eq. (34) with the applied vector potential $A=-rB_a/2$ inserted, one obtains the sheet current which idealy screens the applied field $B_a=\mu_0H_a$ from the ring (more precisely, it shields the perpendicular *flux* from the hole of the ring and the perpendicular *field* from the ring material),

$$J_s^{\rm ideal}(r)=-\frac{1}{2}H_a\int_{a_1}^{a}dr'\ Q(r,r')^{-1}r'\ . \tag{39}$$

Inserting this into Eq. (32) one obtains the magnetic moment of ideal superconducting thin rings and disks divided by H_a,

$$m'_{\rm ring}(0)=-\frac{\pi}{2}\int_{a_1}^{a}dr\int_{a_1}^{a}dr'\ r^2Q(r,r')^{-1}r'\ . \tag{40}$$

In terms of a discrete grid r_i with weights w_i one may write this explicitly as

$$m'_{\rm ring}(0)\approx-\frac{\pi}{2}\sum_{i,j}\ r_i^2w_i(Q_{ij}w_j)^{-1}r_j\,. \tag{41}$$

Evaluating this double sum as a function of the radius ratio a_1/a of the ring one obtains the limits (18) for full disks and (17) for narrow rings, and the values between these limits. Denoting the ratio of the inner and outer radius by $x=a_1/a$ one gets the explicit formulas,

$$\frac{m'(0)}{-a^3}\approx\begin{cases}\dfrac{8}{3}(1-\frac{1}{9}x^5-0.21x^{10}), & x\leqslant0.95\\[2ex] \dfrac{\pi^2}{8}\dfrac{(1+x)^3}{\ln4\left(\dfrac{1+x}{1-x}\right)-0.614}, & x\geqslant0.9.\end{cases} \tag{42}$$

The expressions (42) describe the correct limits $x\ll1$ and $1-x\ll1$; their relative error is <0.001 for $x<0.9$ and <0.01 (0.003, 0.001) for $x>0.9$ (0.95, 0.975), cf. Fig. 2 and

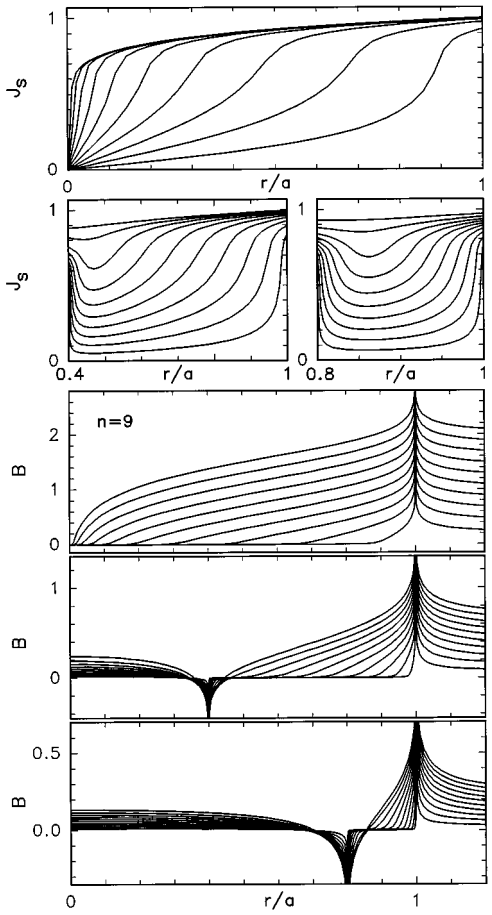

FIG. 8. Same as Fig. 6 for constant J_c and constant ramp rate $\dot{B}_a = 2E_c/a$ but for finite creep exponent $n=9$.

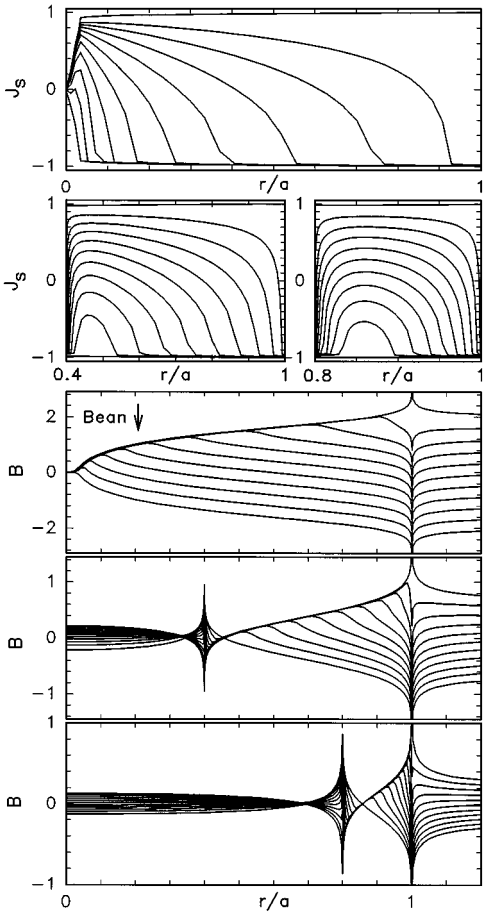

FIG. 9. Same as Fig. 6 but in applied field decreasing with constant ramp rate from H_p to $-H_p$ in steps of $0.2H_p$.

Table I. The excellent fit over many decades suggests that the factor $1-0.111x^5$ in Eq. (42) presents the exact limiting behavior for $x \ll 1$, which should be derivable analytically. Also it seems likely that the exact value of the constant 0.614 should be $2-\ln 4 = 0.614$. A general interpolation formula with relative error $<2\%$ for all radius ratios $0 \leqslant x = a_1/a < 1$ is

$$\frac{m'_{\rm ring}(0)}{-a^3} = \frac{2.064 + 5.351x + 2.456x^{3.5}}{\ln\left[16\left(\frac{1+x}{1-x}\right)\right] - 2} . \qquad (43)$$

Note that the initial slope $m'(0)$ does not depend on the creep exponent n as long as $n>1$: The nonlinearity of $E \propto J^n$ guarantees that in the limit of small H_a, and thus small J, any nonlinear conductor is an ideal conductor which screens perfectly.

B. Field of full penetration

The computation of the field of full penetration $H_p^{\rm ring}$ for rings with arbitrary radius ratio $0 \leqslant x = a_1/a < 1$ and finite creep exponent n requires time integration of Eq. (30). Using constant ramp rate $\dot{B}_a$ and a large creep exponent $n \gg 1$ one is still left with some arbitrariness in defining H_p since for finite n the magnetic saturation is reached only gradually, see Eq. (27). One possible definition of H_p by monitoring the vanishing spatial variation of the current density $J(\mathbf{r},t)$ was used in Ref. 14. Here I use a slightly different definition in terms of the magnetization curve $m(H_a)$. The computed function $f(H_a) = \ln(\partial m/\partial H_a)$ performs a rather sharp bend from a nearly horizontal line at $H_a \leqslant H_p$, where $\partial m/\partial H_a \approx m'(0)$, to a steeply decreasing straight line at $H_a > H_p$, which reflects the exponentially decreasing slope of $m(H_a)$, Eq. (27). Here I define H_p as the H_a value at this bend.

To obtain the Bean limit $n \to \infty$ by this method I used $n=200$ and $\dot{B}_a = 2E_c/a$, or $\dot{B}_a = 1$ in units $a = 2E_c = J_c d = 1$. The penetration field $H_p^{\rm ring}$ computed in this way is in good agreement (relative error $<1\%$) with the exact value obtained directly from the integral kernel $Q(r,r')$ in the following way.

Looking at the profiles of the perpendicular magnetic field $B_z(r)$ in the ring plane $z=0$ during increase of the applied field H_a, Fig. 6, one notes that magnetic flux enters the ring material from the outer and inner edges. As long as the penetrating flux fronts (which in this transverse geometry exhibit vertical slopes[4–8]) have not yet met, there is a field-free zone with $B_z = 0$ between these two fronts. When H_a has reached the value $H_p^{\rm ring}$, the flux fronts meet at $r = r_p$ and the sheet current J_s saturates to the value $J_c d$. At this moment, there is still no flux in the circular zone $r \leqslant r_p$, thus,

$$\int_0^{r_p} 2\pi r B_z dr = 2\pi r_p A(r_p) + \pi r_p^2 B_p = 0 . \qquad (44)$$

TABLE I. The initial slope $m'_{\rm ring}(0)$ [Eq. (40)] of the magnetization curve of a thin superconducting ring, the field of full penetration H_p [Eq. (45)] of this ring in the Bean model, and the penetration radius r_p where the flux fronts meet in the ring, as functions of the ratio a_1/a of the inner and outer radius.

a_1/a	$-[m'(0)/a^3]$	H_p/J_cd	r_p/a
0.005	2.6667	2.8825	0.00583
0.010	2.6667	2.5359	0.01166
0.025	2.6667	2.0777	0.02913
0.050	2.6667	1.7309	0.05830
0.100	2.6667	1.3833	0.11639
0.150	2.6667	1.1790	0.17439
0.200	2.6666	1.0328	0.23210
0.300	2.6659	0.8235	0.34617
0.400	2.6634	0.6699	0.45782
0.500	2.6561	0.5452	0.56609
0.600	2.6381	0.4365	0.66984
0.700	2.5977	0.3365	0.76765
0.800	2.5089	0.2389	0.85762
0.850	2.4283	0.1888	0.89890
0.900	2.2998	0.1360	0.93693
0.950	2.0682	0.0776	0.97112
0.980	1.7851	0.0365	0.98925
0.990	1.6030	0.0204	0.99479
0.995	1.4488	0.0113	0.99744
0.999	1.1770	0.0028	0.99950

Here I used $rB_z=\partial(rA)/\partial r+rB_a$ and $B_a=B_p=\mu_0H_p$. The current-caused vector potential $A(r)$ in the plane $z=0$ is given by Eq. (34) with $J_s(r)=J_cd=$const inserted. Thus we get the condition for flux conservation,

$$\frac{H_p}{J_cd}=-\frac{2}{r}\int_{a_1}^{a}Q(r,r')\,dr' \quad \text{at } r=r_p. \tag{45}$$

In order to determine the two unknown variables H_p and r_p we need a second equation, e.g., the condition $B_z(r_p)=0$, which is obvious when the flux fronts meet at $r=r_p$. We note in passing that one has $B_z(r_p)=0$ for $H_a\leqslant H_p$ and, since the current has saturated, $B_z(r_p)=H_a-H_p$ for $H_a\geqslant H_p$. Using $B_z=(1/r)(\partial/\partial r)(rA)+B_a$ and the expression (34) for $A(r)$ with $J_s=J_cd$ at $r=r_p$ when $B_a=\mu_0H_p$, one obtains the second condition,

$$\frac{H_p}{J_cd}=-\frac{1}{r}\frac{\partial}{\partial r}r\int_{a_1}^{a}Q(r,r')\,dr' \quad \text{at } r=r_p. \tag{46}$$

Instead of calculating H_p and r_p from Eqs. (45) and (46) I use a more elegant, accurate, and faster way of maximizing a function which has its maximum value H_p at $r=r_p$. Namely, one can show that Eq. (46) is equivalent to the condition $(\partial/\partial r)(1/r)\int Q(r,r')dr'=0$ when Eq. (45) holds. Therefore, one may obtain both H_p and r_p for the ring in the Bean state in one step from the maximum problem

$$H_p^{\rm ring}=\max\left(-\frac{2}{r}\int_{a_1}^{a}Q(r,r')\,dr'\right)J_cd\ . \tag{47}$$

The resulting H_p values (Table I, Fig. 3) agree well with the limiting expressions for $x=a_1/a\ll 1$, obtained by putting $d\approx 5a_1$ in Eq. (11), and for $x\approx 1$, Eq. (16).

Very accurate fits with relative error $<10^{-5}$ for $a_1/a\geqslant 0.999$ are obtained if in Eq. (16) the constant c, which in the discussion following Eq. (14) was chosen to equal 1/2, is chosen as $c=0.307=1-\ln 2$. The reason for this different c value is the ambiguity of the definition of the self-inductivity L of a ring:[42] The constant $c=1/2$ is obtained when one defines L via the energy $\frac{1}{2}LI^2$ of the currents in a flat ring with constant current density $J=J_c$; this yields for L a double integral over the ring width w since all circular current paths interact with each other. However, in the present problem of finding the field of full penetration, a different definition of L is appropriate, namely, via the flux $\phi=LI$ in the ring as mentioned before Eq. (15). The radius of the circle inside which this flux is enclosed, depends on the specific problem. Here it means the radius r_p at which the two flux fronts meet. For narrow rings one has $r_p=R=a-w/2$. This definition of L requires a single integral over the ring width and yields $L=\phi(R)/I=\mu_0[\ \ln(16R/w)-1\ ]$, i.e., Eq. (14) with $c=1-\ln 2$.

Explicitly I find the limits

$$\frac{H_p^{\rm ring}}{J_cd}\approx\begin{cases}\dfrac{1}{2}(-\ln x+0.467), & x\leqslant 0.6\\[2ex] (2/\pi)\left(\dfrac{1-x}{1+x}\right)\left(\ln 4\left(\dfrac{1+x}{1-x}\right)-0.307\right), & x\geqslant 0.8,\end{cases} \tag{48}$$

with relative error $<1\%$. A good interpolation to the entire range $0\leqslant x<1$ with relative deviation $<2\%$ is

$$\frac{H_p^{\rm ring}}{J_cd}\approx\frac{2p}{\pi}\left(\ln\frac{8}{p}-1\right)-\frac{1}{2}(\ln x+1-x) \tag{49}$$

with $p=(1-x)/(1+x)=w/(2R)$, $x=a_1/a=(2R-w)/(2R+w)$. Note that expresssion (49) contains *no fit parameter* and yields the correct limits for both $x\to 0$ and $x\to 1$.

C. Computed magnetization curves

Approximate Bean magnetization curves for thin rings with arbitrary inner and outer radii a_1 and a may be constructed from the initial slope (43), the penetration field (49), and the saturation moment (26), using the $m(H_a)$ expressions (9) and (12) for disks and narrow rings and the prescription (1) to generate the full hysteresis loop from the virgin curve. Alternatively, one can compute the magnetiza-

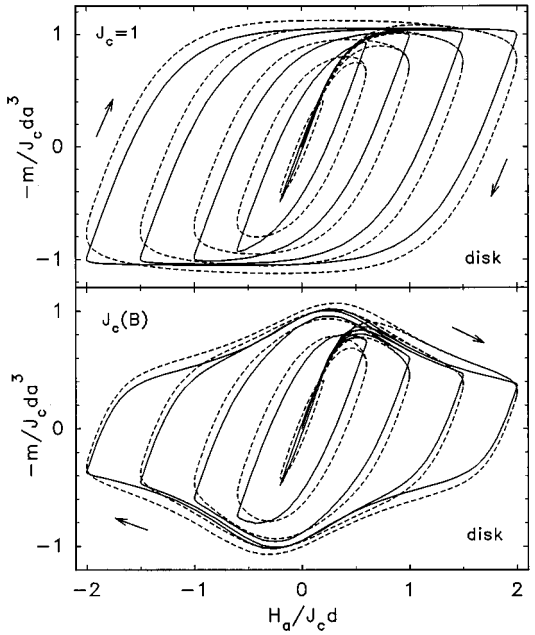

FIG. 10. Theoretical magnetization curves $m(H_a)$ of a thin disk (radius a) with $J_c=$ const (top) and $J_c=J_c(B)=J_c(0)/(0.8+|B|)$ (bottom), B is in units $\mu_0 J_c d$, m in units $J_c d a^3$. Solid lines: Weak creep, $n=51$ (Bean and Kim models). Dashed lines: Strong creep, $n=5$ in $E(J,B)=E_c[J/J_c(B)]^n$. The curves for $n=11$ would lie in the middle between the curves $n=5$ and $n=51$. The applied field is cycled sinusoidally, $H_a(t)=H_0\sin\omega t$ with $\omega=2E_c/(\mu_0 J_c da)$, starting at time $t=0$. The stationary hysteresis loop is reached before the first cycle is completed.

tion curves directly from Eqs. (30) to (32), considering also creep and a field dependent $J_c(B)$.

Such computed magnetization curves are depicted in Figs. 10 and 11 for the Bean limit ($n=51$) and for strong creep ($n=5$) for the thin disk and a ring with radius ratio $a_1/a=0.6$. The upper plots show the Bean model $J_c=$ const, and the lower plots the Kim model $J_c(B)=J_c(0)/(0.8+|B|)$ with B in units $\mu_0 J_c d$. The applied field is cycled sinusoidally, $H_a(t)=H_0\sin\omega t$ with $\omega=2E_c/(\mu_0 J_c da)$. Shown are the virgin curves and hysteresis loops for amplitudes $H_0/J_c d=0.2$, 0.6, 1, 1.5, and 2. Note that even this wide ring exhibits almost parallelogram-shaped hysteresis loops, which are typical for a narrow ring, cf. Eqs. (1) and (2).

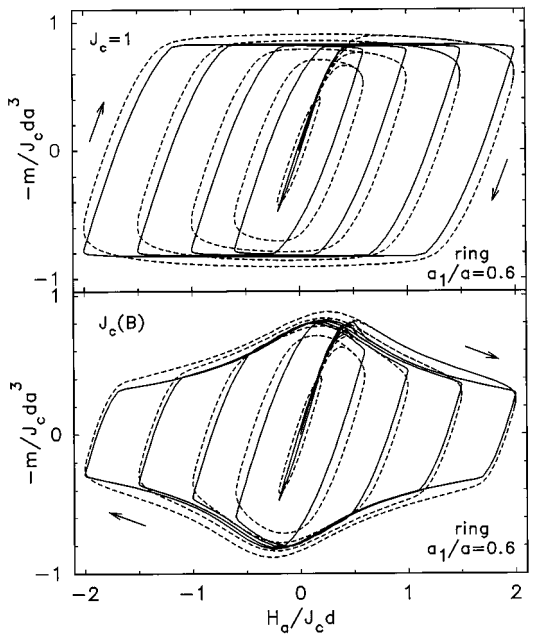

FIG. 11. Same as Fig. 10 but for a thin ring with radius ratio $a_1/a=0.6$.

With decreasing creep exponent n the magnetization curves become more rounded, and for $n=1$ they become ellipses, as expected for an ohmic conductor with constant resistivity. The computed magnetization curves and susceptibilities exactly satisfy the scaling law of Sec. VI B. Namely, the same curves result, e.g., if we increase the frequency by a factor of 1000 and increase our field and current units by a factor of $1000^{1/(n-1)}$.

For $n\gg 1$ the upper and lower slightly curved parts of the hysteresis loops can be calculated by assuming that the current has saturated to $|J|\approx J_c$, see Sec. V. This yields $\nabla\times\mathbf{E}\approx-\dot{\mathbf{B}}_a=\hat{\mathbf{z}}\omega\mu_0 H_0\cos\omega t=\pm\hat{\mathbf{z}}\omega\mu_0(H_0^2-H_a^2)^{1/2}$, thus $|E(r,t)|\approx(r/2)|\dot{B}_a|=(r/2)\omega\mu_0(H_0^2-H_a^2)^{1/2}$. With $|J(r,t)|=J_c|E(r,t)/E_c|^{1/n}$ one then obtains the magnetic moment of the upper and lower branches of $m(H_a)$,

$$m(H_a)\approx\pm m_{\rm sat}(1-H_a^2/H_0^2)^{1/(2n)} \tag{50}$$

with the saturation value $m_{\rm sat}$ from Eq. (25) with $\dot{B}_a=\omega\mu_0 H_0$ inserted. This approximation indeed fits the computed curves within line thickness in the interval $0\leqslant H_a\,\mathrm{sgn}(\dot{H}_a)\leqslant H_0$. Its derivation shows that the slight decrease of the magnetic moment $m(H_a)$ following the steep increase of the virgin curve, is not an indication of flux creep but is due to the decrease of the ramp rate $\dot{B}_a=\mu_0\dot{H}_a$ after $H_a(t)$ has reached its maximum.[38]

D. Nonlinear susceptibilities

Figures 12 and 13 show the nonlinear susceptibilities $\chi(H_0)=\chi'-i\chi''$ obtained from the magnetization loops of Figs. 10 and 11 for the disk and a ring for creep exponents $n=3$, 5, 11, and 51 in the current-voltage law $E(J,B)=E_c[J/J_c(B)]^n$. With decreasing n (increasing creep) $\chi'(H_0)$ is reduced and $\chi''(H_0)$ enhanced at all ac amplitudes H_0, and the maximum of $\chi''(H_0)$ increases and is shifted to lower H_0. Accounting for the decrease of $J_c(B)$ with increasing local field B, also modifies the susceptibility, cf. the dashed curves in Figs. 12 and 13: At large amplitudes $H_0\gg H_p$ both χ' and χ'' are reduced, while near H_p, χ' is reduced but χ'' enhanced, and the maximum of χ'' (the dissipation maximum) is shifted to lower ac amplitudes.

VIII. SUMMARY AND CONCLUSIONS

The magnetization curve and nonlinear ac susceptibility of narrow type-II superconductor rings in a perpendicular field are derived for constant critical current density J_c (Bean model), Eq. (20). This result is then generalized (a) to rings of arbitrary hole diameter, (b) to finite resistivity causing flux creep, (c) to nonconstant $J_c(B)$ (e.g., the Kim model), and (d) to thick rings and disks. The exact formulation of this

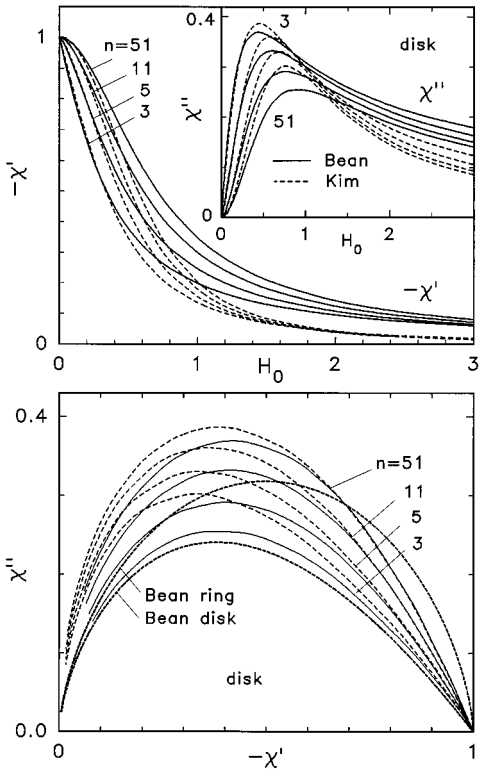

FIG. 12. Nonlinear susceptibility $\chi(H_0)=\chi'-i\chi''$ of a disk. Same case as in Fig. 10, but for creep exponents $n=3$, 5, 11, and 51. H_0 is in units $J_c d$. Solid lines: $J_c=$const. Dashed lines: $J_c(B)=J_c(0)/(0.8+|B|)$ with B in units $\mu_0 J_c d$. Top: χ' and χ'' versus the ac amplitude H_0 of $H_a(t)=H_0\sin\omega t$, $\omega=2E_c/(\mu_0 J_c d a)$. Bottom: Polar plot χ'' versus $-\chi'$. The dashed lines show the Bean limit for thin disks and narrow rings.

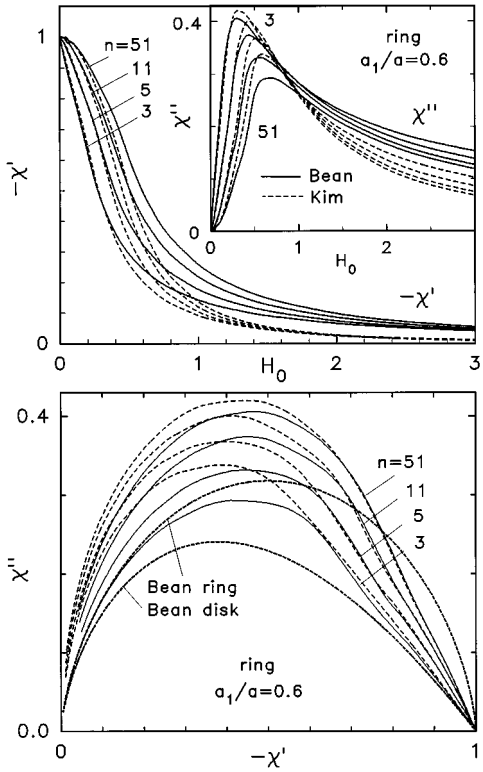

FIG. 13. Same as Fig. 12 but for a thin ring with radius ratio $a_1/a=0.6$.

general problem is given in terms of an integral equation for the current density $J(r,z,t)$ in thick rings (or disks, tubes, cylinders) in axial applied field $H_a(t)$, Eq. (28), and for the sheet current $J_s(r,t)$ in thin rings, Eq. (30). As examples, the current and field profiles, magnetization curves, and nonlinear susceptbilities of thin disks and rings in cycled $H_a(t)$ are computed, accounting also for flux creep and for field dependent $J_c(B)$. Explicit expressions are given for the initial slope (42), penetration field (48), and saturation value (25) of the magnetization curve as functions of the hole radius a_1 and creep exponent n.

Inspection of the equation for $J(r,z,t)$ reveals a scaling law which states that for any current-voltage power-law $E\propto J^n$ the solutions for currents, fields, and magnetic moments remain the same when the time unit and the amplitude of the applied magnetic field are changed simultaneously. In particular, the nonlinear susceptibility in a periodic field $H_a(t)=H_0\sin\omega t$ may be written as $\chi(\omega,H_0)=f(H_0/\omega^{1/\sigma}+\omega/H_0^{\sigma})$, where $\sigma=n-1$ and f is a universal function depending only on the geometry. This means that $\chi=\chi(\omega)$ for $n\to 1$ (Ohm) and $\chi=\chi(H_0)$ for $n\to\infty$ (Bean).

The distribution of $\mathbf{B}(\mathbf{r},t)$ and $\mathbf{J}(\mathbf{r},t)$ inside a real, three-dimensional type-II superconductor calculated from Eq. (28), may be used to compute the observed ''giant magnetostriction''[43] or ''suprastriction.''[44] This magnetomechanical effect is caused by surface screening currents and the Lorentz force density $\mathbf{B}\times\mathbf{J}$ exerted by the local current density $\mathbf{J}$ on the flux lines and then transferred to the atomic lattice via flux-line pinning. The method may also be used to calculate the levitation force on cylindrical (or any rotationally symmetric) superconductors above or below a magnet,[45] and the frequency shift and damping of vibrating superconductors in a magnetic field.[46] The ac susceptibility of narrow rings has recently been measured in detail[47,48] and closely fits formula (20).

ACKNOWLEDGMENTS

Helpful discussions with Alexander Gurevich, John Gilchrist, Pablo Esquinazi, Paul Ziemann, Alexander Forkl, Christian Jooss, Michail Indenbom, and Igor Landau are gratefully acknowledged.

[1] C.P. Bean, Phys. Rev. Lett. **8**, 250 (1962); Rev. Mod. Phys. **36**, 31 (1964).
[2] A.M. Campbell and J.E. Evetts, Adv. Phys. **21**, 199 (1972).
[3] E.H. Brandt, Phys. Rev. B **52**, 15 442 (1995).
[4] W.T. Norris, J. Phys. D **3**, 489 (1970); Y. Yang, T. Hughes, C. Beduz, D.M. Spiller, R.G. Scurlock, and W.T. Norris, Physica C **256**, 378 (1996).
[5] E.H. Brandt, M. Indenbom, and A. Forkl, Europhys. Lett. **22**, 735 (1993).
[6] E.H. Brandt and M. Indenbom, Phys. Rev. B **48**, 12 893 (1993).

[7] E. Zeldov, J. R. Clem, M. McElfresh, and M. Darwin, Phys. Rev. B **49**, 9802 (1994).
[8] P.N. Mikheenko and Yu.E. Kuzovlev, Physica C **204**, 229 (1993).
[9] J. Zhu, J. Mester, J. Lockhart, and J. Turneaure, Physica C **212**, 216 (1993).
[10] J.R. Clem and A. Sanchez, Phys. Rev. B **50**, 9355 (1994).
[11] E.H. Brandt, Phys. Rev. Lett. **74**, 3025 (1995).
[12] E.H. Brandt, Rep. Prog. Phys. **58**, 1465 (1995).
[13] A. Forkl, Phys. Scr. **T49**, 148 (1993).
[14] E.H. Brandt, Phys. Rev. B **54**, 4246 (1996).
[15] E.H. Brandt, Phys. Rev. B **49**, 9024 (1994); Phys. Rev. Lett. **71**, 2821 (1993).
[16] A.T. Dorsey, Phys. Rev. B **51**, 15 329 (1995).
[17] E.H. Brandt, Phys. Rev. B **50**, 4034 (1994).
[18] E.H. Brandt, Physica C **235-240**, 2939 (1994).
[19] Th. Schuster, H. Kuhn, E.H. Brandt, M. Indenbom, M.V. Koblischka, and M. Konczykowski, Phys. Rev. B **50**, 16 684 (1994).
[20] Th. Schuster, M.V. Indenbom, H. Kuhn, E.H. Brandt, and M. Konczykowski, Phys. Rev. Lett. **73**, 1424 (1994).
[21] J. Gilchrist and E.H. Brandt, Phys. Rev. B **54**, 3530 (1996).
[22] L.D. Landau and E.M. Lifshitz, *Electrodynamics of Continuous Media*, Vol. III of Theoretical Physics (Pergamon, Oxford, 1963).
[23] Such parallelograms are obtained also in rings with a weak link (Ref. 24) and in other models; see the discussion by Gilchrist (Ref. 25 and the references therein).
[24] T. Ishida and H. Mazaki, J. Appl. Phys. **52**, 6798 (1981).
[25] J. Gilchrist and M. Konczykowski, Physica C **212**, 43 (1993).
[26] R.W. Rollins and J. Silcox, Phys. Rev. **155**, 404 (1967); H.J. Fink, *ibid.* **161**, 417 (1967); D. de Klerk and C.A.M. van der Klein, J. Low Temp. Phys. **6**, 1 (1972).
[27] T. Ishida, R.B. Goldfarb, S. Okayasu, Y. Kazumata, J. Franz, T. Arndt, and W. Schauer, Mater. Sci. Forum **137-139**, 103 (1993).
[28] M.V. Feigel'man, V.B. Geshkenbein, A.I. Larkin, and V.M. Vinokur, Phys. Rev. Lett. **63**, 2303 (1989); T. Nattermann, *ibid.* **64**, 2454 (1990).
[29] D.S. Fisher, M.P.A. Fisher, and D.A. Huse, Phys. Rev. B **43**, 130 (1991); A.T. Dorsey, *ibid.* **43**, 7575 (1991).
[30] G. Blatter, M.V. Feigel'man, V.B. Geshkenbein, A.I. Larkin, and V.M. Vinokur, Rev. Mod. Phys. **66**, 1125 (1994).
[31] J. Rhyner, Physica C **212**, 292 (1993).
[32] J. Gilchrist and C.J. van der Beek, Physica C **231**, 147 (1994).
[33] A. Gurevich and H. Küpfer, Phys. Rev. B **48**, 6477 (1993).
[34] A. Gurevich and E.H. Brandt, Phys. Rev. Lett. **73**, 178 (1994).
[35] A. Gurevich, Int. J. Mod. Phys. B **9**, 1045 (1995).
[36] E.H. Brandt, Phys. Rev. Lett. **76**, 4030 (1996).
[37] J. McDonald and J.R. Clem, Phys. Rev. B **53**, 8643 (1996).
[38] A. Gurevich (private communication).
[39] E.H. Brandt (unpublished).
[40] V.B. Geshkenbein, M.V. Feigel'man, and V.M. Vinokur, Physica C **185-189**, 2511 (1991).
[41] E.H. Brandt and A. Gurevich, Phys. Rev. Lett. **76**, 1723 (1996); A. Gurevich and E. H. Brandt, Phys. Rev. B **55**, 12706 (1997).
[42] J. Gilchrist (private communication).
[43] H. Ikuta, N. Hirota, Y. Nakayama, K. Kishio, and K. Kitazawa, Phys. Rev. Lett. **70**, 2166 (1993).
[44] H. Kronmüller, Phys. Status Solidi **40**, 295 (1970).
[45] E.H. Brandt, Science **243**, 349 (1989).
[46] M. Ziese, P. Esquinazi, and H.F. Braun, Supercond. Sci. Technol. **7**, 869 (1994).
[47] F. Mrovka, M. Wurlitzer, P. Esquinazi, E.H. Brandt, M. Lorenz, and K. Zimmer, Appl. Phys. Lett. **70**, 898 (1997).
[48] Th. Herzog, H. A. Radovan, P. Ziemann, and E. H. Brandt, Phys. Rev. B (to be published).